Observation of Temperature-Dependent Transport in the TFTR Tokamak

P. C. Efthimion, D. K. Mansfield, B. C. Stratton, E. Synakowski, A. Bhattacharjee,[(a)] H. Biglari, P. H. Diamond,[(b)] R. J. Goldston, C. C. Hegna,[(a)] D. McCune, G. Rewoldt, S. Scott, W. M. Tang, G. Taylor, R. E. Waltz,[(c)] R. M. Wieland, and M. C. Zarnstorff

Princeton Plasma Physics Laboratory, Princeton, New Jersey 08544

(Received 4 September 1990)

Local particle and heat transport coefficients have been measured in a temperature scan of neutral-beam–heated plasmas with n, I_p, and B_φ held constant. The electron transport is ascertained from a flux analysis of a small density perturbation, and the heat transport is obtained from the equilibrium power balance. The transport coefficients vary as T_e^α, where $\alpha = 1.5$–2.5. The observed temperature dependence is predicted by numerical calculations of anomalous transport due to trapped-particle drift-type microinstabilities.

PACS numbers: 52.55.Pi, 52.25.Fi, 52.55.Fa

Auxiliary-heated plasmas are particularly interesting because of the variety of regimes (e.g., L mode, H mode, supershot) that have been identified. For L-mode plasmas the global confinement has been characterized on many tokamaks, and empirical global scaling laws have been developed.[1–4] These plasmas exhibit a degradation of global confinement with increasing heating power ($\tau \propto P^{-0.6}$). However, the transport mechanism has not been identified. Elecrostatic drift-type microinstability transport theory predicts this confinement degradation due to its strong temperature dependence. Examples of approximate analytical forms of the theory[5] for several instabilities are

$$D_{\rm DTE} = \varepsilon^{1.5}(\rho_s C_s/L_n)^2/\nu_{ei} \propto \varepsilon^{1.5} T_e^{3.5}/nL_n^2 \quad \text{for } \nu_{\rm eff}/\omega^* \gg 1\,,$$

$$D_{\rm CTE} = 3\varepsilon^{0.5}\rho_s^2 C_s/L_n \propto \varepsilon^{0.5} T_e^{1.5}/L_n \quad \text{for } \nu_{\rm eff}/\omega^* \ll 1\,,$$

$$D_{\rm ITG} = \varepsilon^{0.5}(\rho_s C_s)^2 L_s/\nu_{\rm eff} L_{Ti}^3 \propto \varepsilon^{0.5} T_e^{3.5} L_s/L_{Ti}^3\,,$$

where $D_{\rm DTE}$, $D_{\rm CTE}$ are estimates of the diffusivities for the dissipative[6] and collisionless trapped-electron mode;[7] $D_{\rm ITG}$ represents a sheared-slab model estimate of the diffusivity for the ion-temperature-gradient–driven mode[8] in the dissipative trapped-electron regime of collisionality; ρ_s is the ion Larmor radius using the electron temperature; C_s is the sound speed; L_n, L_{Ti}, and L_s are the density gradient, ion-temperature gradient, and shear scale lengths; T_e is the electron temperature; n is the electron density; ν_{ei} is the electron-ion collision frequency; $\nu_{\rm eff} = \nu_{ei}/\varepsilon$; ε is the inverse aspect ratio; and ω^* is the diamagnetic drift frequency. These expressions are typical representations of transport coefficients using mixing-length estimates. The analytic expressions for $D_{\rm DTE}$ and $D_{\rm CTE}$ are strictly applicable at the two extreme limits of collisionality. However, many plasmas including those with L-mode confinement have $\nu_{\rm eff}/\omega^* \approx 1$. Drift-wave and trapped-electron mode theory has been extended to include the dissipative contributions from electrons in three collisionality regimes.[9] Furthermore, a recent model[10] for trapped-electron transport in this regime of collisionality interpolates the T_e and L_n dependences between the two regimes based upon $\nu_{\rm eff}/\omega^*$ and L_n itself. All of the electrostatic drift-type microinstability theories have temperature as a fundamental parameter. Therefore knowledge of the temperature dependence may provide insight into the transport mechanism, and select applicable theories. In this paper the dependence of heat and particle transport on temperature for L-mode plasmas is examined.

Examination of the temperature dependence requires variation of the temperature with all other quantities held constant. In this experiment, a neutral-beam power scan was completed with the final line-integrated density held constant by adjusting the injection target electron density at each power level. Helium gas was applied to the target plasmas to obtain broad density profiles and to ensure L-mode plasma confinement. The neutral beams are injected countertangential and cotangential to the plasma current and fuel the plasma with deuterium neutrals with a maximum energy near 100 keV. Four beam powers ($P_b = 0$, 4.5, 9.0, and 14 MW) were used with the power in the cotangential and countertangential beam sources balanced to minimize plasma rotation. The toroidal magnetic field $B_\varphi = 4.0$ T, the major radius $R = 2.58$ m, the minor radius $a = 0.93$ m, the safety factor $q = 5.1$, and the plasma current $I_p = 1.5$ MA were also held constant. The $Z_{\rm eff}$ increased from 2.8 to 3.6 with beam power. Figure 1 shows the four electron density and temperature profiles achieved in the scan, measured by a ten-channel far-infrared interferometer[11] and by electron-cyclotron-emission radiometry, respectively. With very similar density profiles, the central electron temperature varied by a factor of 2. The location of the sawtooth inversion radius at $r = 0.23$ m was measured from the electron cyclotron emission. The ratio of T_i/T_e increased from 0.8 to 1.25 with input power. The global energy confinement time for plasmas in increasing order of input power were 0.27, 0.127, 0.105, and 0.100 s. The confinement times were, on the average, 1.1 times the L-

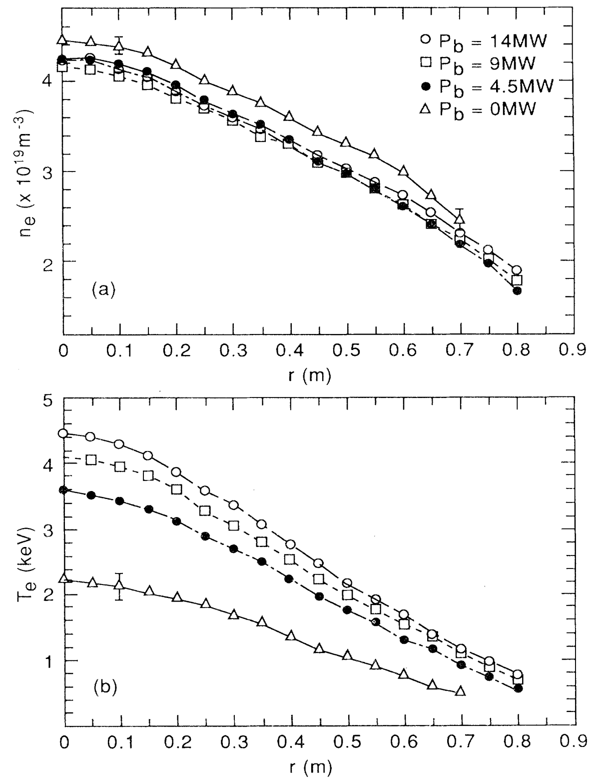

FIG. 1. Electron density and temperature profiles at four neutral-beam–heating powers (0, 4.5, 9, 14 MW).

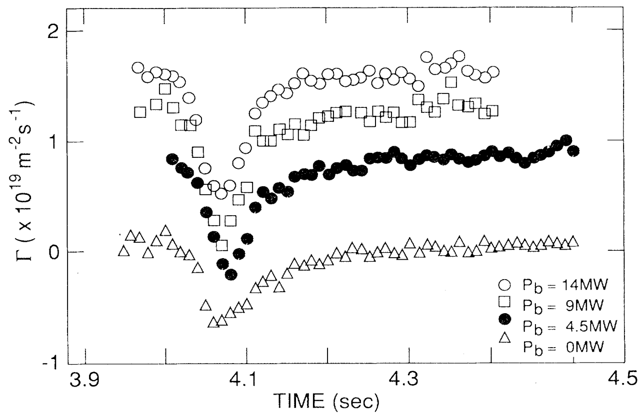

FIG. 2. The time evolution of the electron particle flux Γ at plasma radius $r=0.6$ m at the four neutral-beam–heating powers ($P_b=0$, 4.5, 9.0, 14.0 MW). A gas puff applied at 4.0 s reduces the flux in all cases.

mode confinement scaling.[1] The 1.0-s neutral-beam–heating duration is 4–10 energy confinement times.

A small amount of helium gas (15 torr liter/s for 0.05 s) is puffed into these plasmas to determine the particle transport from the evolution of the density profile using perturbation analysis techniques. The time-dependent profile data, the neutral-beam fueling rate, and the edge wall source are used to solve for the electron particle flux $\mathbf{\Gamma}$ from the particle balance equation: $\partial n/\partial t = -\nabla\cdot\mathbf{\Gamma} + S$, where S is the total electron source as a function of time and radius. The neutral-beam fueling rate profile is calculated with a Monte Carlo beam deposition algorithm,[12] and the wall source is calculated from the total number of particles in the plasma and an estimate of the particle confinement time of 0.1 s. For some of the plasmas the wall source is also compared to the D_α emission. Figure 2 shows $\Gamma(t)$ at a minor radius of $r=0.6$ m for the four power conditions. The gas puff is put in at 4.0 s, and the outward flux decreases in each case due to the density perturbation. Small gas puffs in this experiment produce $\delta n/n \approx 0.07$, $\delta\nabla n/\nabla n \approx 0.2$, $\delta T_e/T_e \approx 0.02$, and $\delta\Gamma/\Gamma \approx 0.3$–$2.0$. The amount of time for the flux to return to equilibrium from its minimum value is indicative of the transport time and the particle transport coefficients. Note that there is a reduction in this recovery time between the low-temperature Ohmically heated plasma ($P_b=0$ MW) and the highest-temperature neutral-beam-heated plasma. The majority of the change in the transport time is observed between the Ohmic and 4.5-MW neutral-beam–heated plasmas. The recovery time and the electron temperature for the 9.0- and 14.0-MW cases look nearly identical. The same observations can be made in comparing the global energy confinement times for these plasmas. Thus, temperature dependence can be seen in the particle flux in Fig. 2.

The particle transport coefficients in previous experiments were determined by fitting the flux with the form $\Gamma(r,t) = -D(r)\nabla n(r,t) + V(r)n(r,t)$, where D and V are assumed constant over the time of the perturbation.[13–16] However, examination of the linearized equation for the perturbed flux including nonconstant transport coefficients indicates that the use of the above flux form leads to erroneous conclusions regardless of the perturbation size.[17] The perturbed flux $\delta\Gamma$ is linearized as

$$\delta\Gamma = [-\langle D\rangle - (\partial D/\partial\nabla n)\langle\nabla n\rangle + (\partial V/\partial\nabla n)\langle n\rangle]\delta\nabla n + [\langle V\rangle + (\partial V/\partial n)\langle n\rangle - (\partial D/\partial n)\langle\nabla n\rangle]\delta n\,,$$

where $\langle\,\rangle$ refers to equilibrium values and δ designates perturbed terms. If D is proportional $1/L_n^\alpha$, where $\alpha\neq 0$, then the term multiplying $\delta\nabla n$ is not just a function of the equilibrium diffusivity $\langle D\rangle$, but also has a contribution from the perturbed diffusivity, $(\partial D/\partial\nabla n)\langle\nabla n\rangle \approx \langle D\rangle$. The assumption that D is constant over the time of the perturbation leads to an error in estimating the magnitude of D, and it should not be compared with the equilibrium value.[17] The term multiplying δn is frequently referred to as the equilibrium pinch term, but it has a contribution from the diffusivity, $(\partial D/\partial n)\langle\nabla n\rangle$, as well as an equilibrium value. If D is proportional to $1/L_n^\alpha$, where $\alpha > 0$, then failing to account for the term

$(\partial D/\partial n)\langle \nabla n\rangle$ leads to the conclusion that the equilibrium pinch is highly anomalous, and the pinch flux $\approx$ diffusive flux. The pinch has to be reconciled from the equilibrium balance, or some alternative analysis technique.

Here a general flux expression is adopted that allows for nonlinear transport coefficients: $\delta\Gamma = (\partial\Gamma/\partial\nabla n)\delta\nabla n + (\partial\Gamma/\partial n)\delta n$, where the partial derivatives $\partial\Gamma/\partial\nabla n$ and $\partial\Gamma/\partial n$ have the same units as D and V, respectively, and are hereafter referred to as the particle transport coefficients. The values of $\partial\Gamma/\partial\nabla n$ and $\partial\Gamma/\partial n$ are derived from a multiple linear regression of the flux applied at each radius for many time slices during the density perturbation with n and ∇n as independent variables. Multiple regression makes fits to the perturbed portion of each parameter (e.g., $\delta\Gamma, \delta\nabla n, \delta n$), and ignores their steady-state components. Integrating the functional form of $\partial\Gamma/\partial\nabla n$ and $\partial\Gamma/\partial n$ with respect to n and ∇n is necessary to yield the functional dependence of the total flux and the equilibrium transport coefficients, but is not required to observe a temperature dependence.

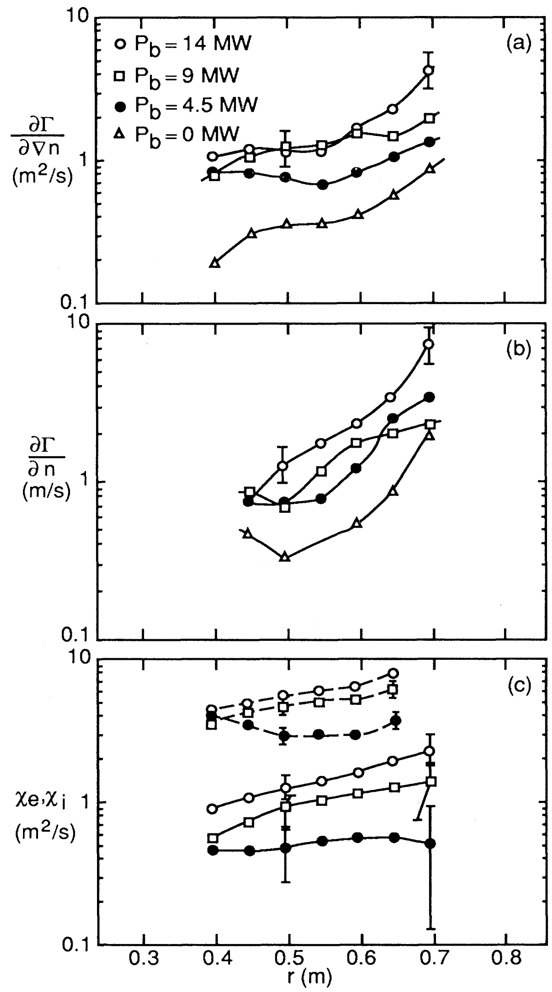

FIG. 3. (a) Particle transport coefficient $\partial\Gamma/\partial\nabla n$ vs plasma radius. (b) Particle transport coefficient $\partial\Gamma/\partial n$ vs plasma radius. (c) Electron and ion thermal diffusivities (χ_e, χ_i) vs plasma radius. The points with dashed lines are χ_i and those with the solid lines are χ_e.

The analysis outlined in the previous paragraph is applied to the particle flux from the temperature scan. It is applied outside the $q=1$ surface to avoid density sawtooth effects, but not within 0.23 m of the last closed flux surface in order to minimize the influence of the edge electron source term in the particle balance, and the radiative power in the heat balance. Figures 3(a) and 3(b) show the particle transport coefficients $\partial\Gamma/\partial\nabla n$ and $\partial\Gamma/\partial n$ as a function of radius for the four plasma cases described in Fig. 1. At each radius there is an increase in the coefficients with increasing electron temperature. In addition there is a radial dependence in the coefficients with smaller values toward the center of the plasma. Previous studies of particle transport using gas puffs have obtained limited information concerning the radial dependence of the transport coefficients.[13-15] The electron and ion thermal conductivities χ_e and χ_i [Fig. 3(c)] are obtained from equilibrium power balance analysis assuming no heat pinch, and exhibit similar temperature and spatial behavior to $\partial\Gamma/\partial\nabla n$ [Fig. 3(a)]. χ_e and χ_i are calculated for the neutral-beam-heated plasmas, which have accurate ion temperature profile measurements using charge-exchange recombination spectroscopy. For these L-mode plasmas $\chi_i > \chi_e$. The thermal diffusivity error bars represent the standard deviation of 100 power balance analyses with the plasma parameters varied within their uncertainties using a Gaussian probability distribution. The particle transport coefficient error bars represent the uncertainties in the wall source, in the density profile measurement, and the standard deviation of the regression fits. A variation by a factor of ± 4 in the wall source results in a 5% uncertainty in the transport coefficient at $r=0.7$ m because the last closed flux surface is 0.23 m from this point.

At each radius the transport coefficients in Fig. 3 are assumed to be proportional to T_e^{α}, and the temperature exponent α is plotted in Fig. 4 as a function of radius. $\partial\Gamma/\partial\nabla n$ and $\partial\Gamma/\partial n$ exhibit the same temperature scaling at each radius, with values of α ranging from 1.5 to 2.5. Similar values of the temperature exponent are obtained for χ_e and χ_i. The uncertainties in determining the temperature dependence of χ_e and χ_i can be reduced by examining a single heat diffusivity for the plasma defined[18] as $\chi_{\rm flux} \equiv -(Q_e+Q_i)/(n_i\nabla T_i + n_e\nabla T_e)$. This avoids the large uncertainties in decoupling the electron and ion heat flows. The temperature dependence of the $\chi_{\rm flux}$ is also shown in Fig. 4, and is similar to the values obtained for the particle transport coefficients $\partial\Gamma/\partial\nabla n$ and $\partial\Gamma/\partial n$.

The temperature exponents observed for the heat and particle transport coefficients are between the values of 1.5 and 3.5 predicted by the analytical forms of trapped-particle drift-type microinstability transport

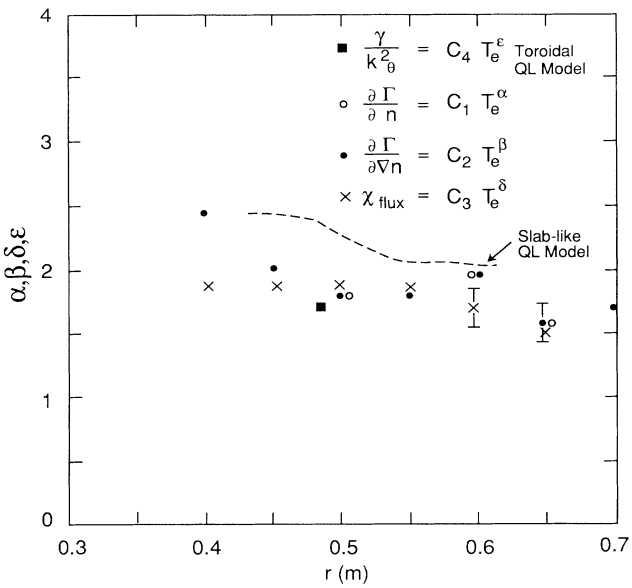

FIG. 4. The electron-temperature exponent of the transport coefficients $\partial\Gamma/\partial\nabla n$, $\partial\Gamma/\partial n$, and χ_{eff}, and a comparison with numerical calculations of the temperature exponents from two driftlike microinstability theories (slablike QL model and toroidal QL model).

theory for the two extremes of collisionality in the banana regime as expected by Ref. 12 for our values of ν_{eff}/ω^*. Two numerical codes were used to predict the temperature exponent from microinstability theory for these plasmas. The first involved comprehensive kinetic microinstability calculations in toroidal geometry for trapped-particle modes driven by trapped-electron and η_i (∇T_i) dynamics.[19] For $r<0.65$ m, $\eta_i>2$ for all of the plasmas, and this calculation indicates that η_i mode behavior should be dominant in this region. The temperature exponents of the transport coefficients expressed in terms of the mode growth rate and the mode wave vector, γ/k_θ^2, are calculated, and the average temperature exponent for the four plasma cases at $r=0.5$ m is shown in Fig. 4 [referred to as the toroidal quasilinear (QL) model]. The average of the calculated values is close to the experimental temperature exponents for heat and particle transport coefficients at the same radius. The calculation also includes examination of the separate fluxes, and indicates that the electron and ion heat diffusivities have the same electron temperature dependence as γ/k_θ^2. This justifies inspection of the single flux χ_{flux} for the temperature dependence. In addition, the average temperature exponent for the four discharges is calculated over the radius $r=0.35$–0.6 m with a slablike quasilinear model of trapped-particle transport (referred to as the slablike QL model) assuming that the η_i mode behavior is dominant.[12] The numerical values are shown as a dashed line in Fig. 4 and are also close to the experimental results.

In summary, a strong temperature dependence has been observed in particle and heat transport coefficients for standard L-mode plasmas. The temperature dependence is predicted by numerical calculations of anomalous transport due to drift-type microinstabilities. The temperature dependence is consistent with, and strongly supports, electrostatic drift-type microinstability transport theory.

It is a pleasure to acknowledge the physicists and staff who support the TFTR program. We would like to acknowledge helpful discussions with S. Cowley, J. B. Taylor, J. Callen, and many of the participants of the Transport Task Force. This work was supported by the U.S. DOE, Contract No. DE-AC02-76-CHO-3073.

[a]Permanent address: Columbia University, New York, NY 10027.

[b]Permanent address: University of California at San Diego, La Jolla, CA 92093.

[c]Permanent address: General Atomics, Inc., San Diego, CA 92138.

[1]R. J. Goldston, Plasma Phys. Controlled Fusion **26**, 87 (1984).

[2]S. M. Kaye, Phys. Fluids **28**, 2327 (1985).

[3]M. Murakami *et al.*, Phys. Rev. Lett. **39**, 615 (1977).

[4]K. H. Burrell *et al.*, Nucl. Fusion **23**, 536 (1983).

[5]D. W. Ross *et al.*, IPSG Panel Report No. DOE/ET-53193-7, 1987 (unpublished).

[6]B. B. Kadomtsev and B. P. Pogutse, Rev. Plasma Phys. **5**, 249 (1970).

[7]J. C. Adam *et al.*, Phys. Fluids **19**, 561 (1976).

[8]P. W. Terry *et al.*, Phys. Fluids B **1**, 109 (1989).

[9]W. Horton, Phys. Fluids **19**, 711 (1976).

[10]R. E. Waltz and R. R. Dominguez, Phys. Fluids **31**, 2920 (1988).

[11]D. K. Mansfield *et al.*, Appl. Opt. **26**, 44679 (1987).

[12]R. J. Goldston *et al.*, J. Comp. Phys. **43**, 61 (1981).

[13]J. D. Strachan *et al.*, Nucl. Fusion **22**, 1145 (1982).

[14]N. L. Vasin *et al.*, Fiz. Plazmy **10**, 918 (1984) [Sov. J. Plasma Phys. **10**, 525 (1984)].

[15]K. W. Gentle *et al.*, Plasma Phys. Controlled Fusion **29**, 1077 (1987).

[16]P. C. Efthimion *et al.*, in *Proceedings of the Twelfth International Conference on Plasma Physics and Controlled Nuclear Fusion Research, Nice, France, 1988* (International Atomic Energy Agency, Vienna, 1989), Vol. 1, pp. 307–321.

[17]K. Gentle, Phys. Fluids **31**, 1105 (1988).

[18]J. P. Christiansen *et al.*, Nucl. Fusion **28**, 817 (1988).

[19]G. Rewoldt and W. M. Tang, Phys. Fluids B **2**, 318 (1990).